

New Power to Measure Supernova ν_e with Large Liquid Scintillator Detectors

Ranjan Laha,¹ John F. Beacom,^{2,3,4} and Sanjib Kumar Agarwalla⁵

¹*Kavli Institute for Particle Astrophysics and Cosmology, Stanford University,
SLAC National Accelerator Laboratory, Menlo Park, CA 94025, USA*

²*Center for Cosmology and AstroParticle Physics (CCAPP),
Ohio State University, Columbus, OH 43210, USA*

³*Department of Physics, Ohio State University, Columbus, OH 43210, USA*

⁴*Department of Astronomy, Ohio State University, Columbus, OH 43210, USA*

⁵*Institute of Physics, Sachivalaya Marg, Sainik School Post, Bhubaneswar 751005, India
rlaha@stanford.edu, beacom.7@osu.edu, sanjib@iopb.res.in*

(Dated: December 29, 2014)

We examine the prospects for detecting supernova ν_e in JUNO, RENO-50, LENA, or other approved or proposed large liquid scintillator detectors. The main detection channels for supernova ν_e in a liquid scintillator are its elastic scattering with electrons and its charged-current interaction with the ^{12}C nucleus. In existing scintillator detectors, the numbers of events from these interactions are too small to be very useful. However, at the 20-kton scale planned for the new detectors, these channels become powerful tools for probing the ν_e emission. We find that the ν_e spectrum can be well measured, to better than $\sim 40\%$ precision for the total energy and better than $\sim 25\%$ precision for the average energy. This is adequate to distinguish even close average energies, e.g., 11 MeV and 14 MeV, which will test the predictions of supernova models. In addition, it will help set constraints on neutrino mixing effects in supernovae by testing non-thermal spectra. Without such large liquid scintillator detectors (or Super-Kamiokande with added gadolinium, which has similar capabilities), supernova ν_e will be measured poorly, holding back progress on understanding supernovae, neutrinos, and possible new physics.

I. INTRODUCTION

If a core-collapse supernova in the Milky Way appears soon, will the neutrino detectors be ready? Yes, in the sense that the supernova will not be missed, as there are many independent detectors. But would this data be complete enough to answer pressing questions? The answer is no, because not all flavors of neutrinos and antineutrinos will be measured well. We might have to wait a few decades more to get the answers.

Only with all six flavors — expected to be emitted with comparable total energies, but with different spectra and time profiles — can we measure the combined neutrino emission, which reveals the change in gravitational binding energy of the stellar core as well as the effects of any novel energy-loss processes [1, 2]. And only with all six flavors can we test how this energy is apportioned, which reveals the density and neutron-to-proton ratio of the collapsing core as well as the effects of neutrino mixing in extreme conditions [3–5].

The Super-Kamiokande detector will detect $\bar{\nu}_e$ with $\sim 10^4$ events, and will be able to reconstruct its spectrum precisely due to the tight connection between observable energy and neutrino energy in $\bar{\nu}_e + p \rightarrow e^+ + n$ interactions with free protons [6, 7]. The IceCube detector, though it cannot measure individual events or spectra, will measure the time profile of the $\bar{\nu}_e$ flux to high precision [8]. The utility of these precise measurements is limited by how well the other flavors can be measured.

The spectra and time profiles of ν_μ , ν_τ , $\bar{\nu}_\mu$, and $\bar{\nu}_\tau$ — generically called ν_x — are expected to be very similar to each other, which considerably simplifies the detection

problem. These flavors can be measured reasonably well, with $\sim 10^2$ events, in scintillator detectors (KamLAND, Borexino, and soon SNO+) through the $\nu + p \rightarrow \nu + p$ channel, which has good spectral fidelity for the high-energy part of the spectrum [9, 10].

The missing link is sufficient sensitivity to ν_e . Interactions with electrons are suppressed by the small electron mass, and interactions with neutrons are suppressed by nuclear binding effects. Though Super-Kamiokande would have $\sim 10^2$ events caused by ν_e , it is difficult to isolate these from other channels, and no other existing detectors would have appreciable numbers of events.

In a previous paper by two of us, we showed how this situation could be significantly improved if Super-Kamiokande adds dissolved gadolinium to enable neutron detection [11]. This would lead to clean identification of the dominant $\bar{\nu}_e + p \rightarrow e^+ + n$ events, making it easier to separate the ν_e events on electrons and nuclei. We showed that the total energy emitted in ν_e and their average energy could each be measured to $\sim 20\%$ precision.

Here we examine how well ν_e could be measured in large liquid scintillator detectors — those that are comparable to the size of Super-Kamiokande and more than an order of magnitude larger than existing scintillator detectors. The JUNO (also known as Daya Bay II) [12, 13] detector is already approved, and the RENO-50 [14], LENA [15] detectors are under consideration. These detectors would have yields of $\bar{\nu}_e + p \rightarrow e^+ + n$ events comparable to that of Super-Kamiokande. Importantly, they would have much larger yields of $\nu + p \rightarrow \nu + p$ events than existing detectors. Most importantly, they would have newly powerful sensitivity to ν_e through in-

interactions with electrons and nuclei. Our presentation below closely follows that of Ref. [11], to make it easier to compare results, but fewer details are given here.

In Sec. II, we describe how supernova ν_e can be detected in liquid scintillator detectors. In Sec. III, we estimate how well the parameters of the incident ν_e spectrum can be determined. We conclude in Sec. IV.

II. SUPERNOVA NEUTRINO DETECTION

We discuss the neutrino spectra expected from a supernova, the neutrino detection channels in liquid scintillator detectors, the likely experimental realities of large liquid scintillator detectors, and our proposed strategies to isolate ν_e .

A. Supernova Neutrino Spectra

We assume that the total energy in neutrinos emitted by the supernova is 3×10^{53} erg and that this is equally divided between all six active flavors of neutrinos and antineutrinos. We take the distance to a typical Milky Way supernova to be 10 kpc [16].

For the spectra, we assume a (normalized) modified Maxwell-Boltzmann form [17, 18]

$$f(E_\nu) = \frac{128}{3} \frac{E_\nu^3}{\langle E_\nu \rangle^4} \exp\left(-\frac{4E_\nu}{\langle E_\nu \rangle}\right), \quad (1)$$

where E_ν and $\langle E_\nu \rangle$ are the neutrino energy and average energy. Compared to a regular Maxwell-Boltzmann form, this has somewhat fewer neutrinos at high energies, so our choice is conservative. Typical average energies for the initial neutrino spectra from numerical supernova models are $\langle E_{\nu_e} \rangle \approx 11 - 12$ MeV, $\langle E_{\bar{\nu}_e} \rangle \approx 14 - 15$ MeV, and $\langle E_{\nu_x} \rangle \approx 15 - 18$ MeV.

Due to neutrino mixing in the supernova [3–5, 19–31] or in the Earth [32–35], the ν_e (or $\bar{\nu}_e$) spectrum could be modified (effectively made hotter) by mixing. As in Ref. [11], we focus on scenarios where the expected temperature hierarchy occurs and where we seek to determine if the ν_e spectrum is affected by mixing or not; other scenarios can be tested separately.

B. Detectable Neutrino Interactions

The neutrino detection channels in a liquid scintillator detector are listed in [15, 36–39]. Liquid scintillator detectors can detect electrons, positrons, photons and non-relativistic protons with near-perfect efficiency above a low energy threshold. The detectable energy of a positron is its kinetic energy plus the energy deposited during annihilation, $2m_e$, whereas the detachable energy for an electron is just its kinetic energy. Due to the large number of photoelectrons produced per MeV, the energy and

position resolution is excellent. Neutrons can be detected with high efficiency via their radiative captures on protons and (rarely) carbon, as discussed below.

Electron antineutrinos $\bar{\nu}_e$ can be detected via the inverse beta interaction with free protons, $\bar{\nu}_e + p \rightarrow e^+ + n$ [6, 7]. The 2.2 MeV photon that results from neutron capture on protons is routinely detected in liquid scintillator detectors like KamLAND [40], Double Chooz [41], Daya-Bay [42], and RENO [43]. The double coincidence signal of e^+ and n means that these events can be individually identified. In water Cherenkov detector like Super-Kamiokande, Gadolinium loading would be required to unambiguously detect this interaction [44].

For the elastic scattering of neutrinos on electrons, we follow the discussion in [11], with the important difference that liquid scintillator detectors have no directionality. The angular cut that can be employed in water Cherenkov detectors to suppress backgrounds is not available in liquid scintillator detectors.

All flavors of neutrinos elastically free protons via the neutral-current interaction. The recoil energy of the scattered proton varies from zero to a maximum value that depends on the square of the incident neutrino energy [9, 10]. To account for quenching of the proton energy, we have taken the Birk's constant to be 0.01 cm/MeV, an indicative value that is similar to the measurements in [45]. The quenching factor in the detector will depend on the scintillator properties. Due to the threshold of a liquid scintillator detector during supernova burst (~ 0.2 MeV), this interaction is only sensitive to the neutrino flavors with the highest average energies [9, 10], and the proton recoil spectrum can be used to reconstruct this neutrino spectrum [10].

There are also important interactions of neutrinos with carbon nuclei. Neutrinos interactions via neutral current can also excite the $J^\pi, T = 1^+, 1$ state in ^{12}C , which then decays spontaneously to the ground state via the emission of a 15.11 MeV gamma-ray photon [46–51]. Electron neutrinos ν_e interact with ^{12}C to produce unstable $^{12}\text{N}_{\text{g.s.}}$ in its ground state:

$$\nu_e + ^{12}\text{C} \rightarrow ^{12}\text{N}_{\text{g.s.}} + e^-. \quad (2)$$

The $^{12}\text{N}_{\text{g.s.}}$ decays with a half-life of 11 msec:

$$^{12}\text{N}_{\text{g.s.}} \rightarrow ^{12}\text{C} + e^+ + \nu_e. \quad (3)$$

The maximum kinetic energy of the positron from the $^{12}\text{N}_{\text{g.s.}}$ decay is ≈ 16.8 MeV. Similarly, electron antineutrinos $\bar{\nu}_e$ interact with ^{12}C to produce unstable $^{12}\text{B}_{\text{g.s.}}$:

$$\bar{\nu}_e + ^{12}\text{C} \rightarrow ^{12}\text{B}_{\text{g.s.}} + e^+. \quad (4)$$

The $^{12}\text{B}_{\text{g.s.}}$ nuclei decays with a half-life of 20.2 msec:

$$^{12}\text{B}_{\text{g.s.}} \rightarrow ^{12}\text{C} + e^- + \bar{\nu}_e. \quad (5)$$

The maximum kinetic energy of the electron from the $^{12}\text{B}_{\text{g.s.}}$ decay is ≈ 12.9 MeV. Both types of charged-current events can be identified by the time and space

coincidence of the scattering followed by a decay, though it is difficult to distinguish the two channels. The cross section of the ν_e on ^{12}C in the relevant energy range has been measured by the LSND collaboration [52] and is in good agreement with theoretical calculations [46–51], as expected because these cross sections depend primarily on the measured $^{12}\text{N}_{\text{g.s.}}$ and $^{12}\text{B}_{\text{g.s.}}$ lifetimes. For these interactions, we use the cross sections tabulated in [46].

In Borexino and Double Chooz, it has been shown that positrons can be separated from electrons via pulse shape discrimination, due to the deposited annihilation energy of the positron [53–56]. The positron is detected via its annihilation energy after ortho-positronium formation (fraction $\sim 45\%$), as this state has a long enough lifetime for detection with present technology. Although this has not yet been demonstrated in KamLAND, it is expected that future large liquid scintillator detectors will have this capability. Para-positronium has a lifetime which is three orders of magnitude shorter than ortho-positronium [56], so it is unrealistic to assume that there will be perfect separation of positrons from electrons. However, even with perfect separation, the contours we calculate below would only improve by a factor of $\sim \sqrt{2}$.

There are also neutrino interactions with ^{12}C that are inelastic in the sense of emitted final-state nucleons; we neglect such channels. The neutral-current interaction can cause $\nu + ^{12}\text{C} \rightarrow \nu' + p + ^{11}\text{B}$. The total number of interactions in a 20 kton detector varies from 3 to 31 for neutrino average energies of 12 MeV to 18 MeV. Although the proton recoil spectrum for this interaction extends to a higher energy than due to neutrino-proton scattering [39], it will be difficult to detect them due to the low number of events. Charged-current interactions can lead to particle-unbound excited states of ^{12}N and ^{12}B [57]. The largest yields are from $\nu_e + ^{12}\text{C} \rightarrow e^- + p + ^{11}\text{C}$ and $\bar{\nu}_e + ^{12}\text{C} \rightarrow e^+ + n + ^{11}\text{B}$. Compared to interactions to the ground states, the number of interactions in a 20 kton liquid scintillator detector is between $\sim 10\%$ and $\sim 40\%$, for incoming neutrino average energies of 12 MeV to 18 MeV respectively. It may be possible to tag the ν_e events by the decays of ^{11}C , as has been demonstrated in Borexino [55]. The $\bar{\nu}_e$ events will be hidden by the large yield of inverse beta interaction on free protons.

Liquid scintillator detectors are also sensitive to neutrino interactions on rare ^{13}C [58, 59]. For ν_e , there is a low threshold of 2.2 MeV, and transitions to the ground and 3.5 MeV excited state of ^{13}C are important. Using the cross sections calculated in [59], we find that the number of interactions expected in a 20 kton liquid scintillator detector is $\sim 10 - 20$, depending on the neutrino average energy. Elaborate consideration of the background is needed to discover this signal [58]. Due to the small number of events, we neglect it.

C. Detector properties

Large liquid scintillator detectors are being planned for a variety of physics reasons. These include determination of the neutrino mass hierarchy, precision measurement of neutrino parameters, detection of supernova neutrinos, solar neutrinos, geoneutrinos, sterile neutrinos, atmospheric neutrinos, nucleon decay, and many other exotic searches [12–15, 37, 60–65].

Due to its main design goal of detecting the neutrino mass hierarchy, a detector like JUNO [12, 13] or RENO-50 [14] has very specific features. JUNO will have an inner volume of 20 kton and RENO-50 is being designed to have an inner volume of 18 kton. We assume that the fiducial volume is 20 kton for supernova detection. Although the fiducial volume of both the detectors will be somewhat smaller than the inner volume, due to the short duration and lower backgrounds during a supernova burst, the fiducial volume during a supernova neutrino search can be almost as large as the inner volume. LENA will have a much larger target mass of liquid scintillator, ~ 50 kton [15], and so the precision of our results would improve by a factor of $\sim \sqrt{2.5} \approx 1.6$.

The JUNO liquid scintillator will be primarily linear alkyl benzene ($\text{C}_6\text{H}_5\text{C}_{12}\text{H}_{25}$) [12, 13]. The energy resolution of both JUNO and RENO-50 is expected to be $\sim 3\%/\sqrt{E/\text{MeV}}$ [13]. We neglect the impact of energy resolution in this work except in the case of the 15.11 MeV monochromatic photon. Due to the intrinsic width of the detectable signals, the effect of the energy resolution can be neglected otherwise.

JUNO will not have added gadolinium, in order to achieve lower radioactivity level and higher transparency [12]. In spite of this, JUNO is expected to have a near-perfect efficiency in detecting neutrons. The mean lifetime of neutron capture on protons depend on the scintillator, e.g., it is $\sim 207 \mu\text{sec}$ in KamLAND [66] and $\sim 260 \mu\text{sec}$ in Borexino [67]. By using a time cut of $0.5 \mu\text{sec}$ to $1000 \mu\text{sec}$, nearly all neutrons are detected in KamLAND. Because detector backgrounds can be neglected during the short time of a supernova burst, a long time cut can be used for neutron detection.

Neutron capture on protons yield a 2.2 MeV gamma-ray photon. In addition to free protons, about 1% of the neutrons will also be captured on carbon which yields a 4.9 MeV photon [67]. The width of these monochromatic photon energies is expected to be 0.044 MeV and 0.066 MeV respectively in JUNO and RENO-50. KamLAND employs an energy cut of 1.8 MeV – 2.6 MeV to detect all the neutron capture events on protons [66]. Due to the superior energy resolution of JUNO, an energy cut of 1.9 MeV – 2.5 MeV will be sufficient. Similarly an energy cut of 4.5 MeV – 5.3 MeV will help in detecting all the neutron capture events on carbon.

In a liquid scintillator detector, the spatial cut for neutron capture on protons is mostly driven by the absorption length of the resulting 2.2 MeV photons and the vertex resolution [66]. A spatial cut of 1.6 m is used

in KamLAND to achieve near perfect capture efficiency from this selection [68, 69]. The position resolution in JUNO or RENO-50 is expected to be much better and hence such a spatial will help capture all the neutron capture events on protons. A different spatial cut is required to capture all the neutron capture events on carbon and we expect that these spatial cuts will ensure detection of all the neutron capture events. The large volume of these detectors imply that the fraction of neutrons leaking out will be negligible.

We expect that the overall neutron capture efficiency in future large liquid scintillator detector to be 100%. KamLAND already has a $\sim 95\%$ efficiency of neutron capture on protons in their search for electron antineutrino from reactors [70]. A future liquid scintillator detector like JUNO or RENO-50 will be at a deeper site [13, 60] and hence will have lower background induced by muons [71, 72]. Since the lifetime of $^{12}\text{N}_{\text{g.s.}}$ is very different from the neutron capture lifetime on protons, the impact of neutron detection inefficiency will be on the constraints from $\nu_e + e^-$ events. We will show the impact of 90%, 95%, 99% and 100% neutron detection efficiency on $\nu_e + e^-$ events. Subsequently we will assume 100% neutron capture efficiency throughout the work.

The detection threshold is determined by the radioactive background in the liquid scintillator detector and the surrounding rock. The energy region below ~ 0.2 MeV is dominated by β decays of ^{14}C nuclei. Pulse shape discrimination can be used to reduce this background but it might still be high compared to neutrino interaction

TABLE I. Expected numbers of events in a 20 kton liquid scintillator detector for a Galactic supernova for different values of the neutrino average energy. The total energy is assumed to be 3×10^{53} erg, divided equally among all flavors, at distance of 10 kpc. The detection threshold during a burst is assumed to be $T_{\text{obs}} = 0.2$ MeV. For neutral current interactions, the numbers of events are for one flavor of ν or $\bar{\nu}$.

Detection channel	12 MeV	15 MeV	18 MeV
$\bar{\nu}_e + p \rightarrow e^+ + n$	3898	4857	5727
$\nu + p \rightarrow \nu + p$	50	139	236
$\bar{\nu} + p \rightarrow \bar{\nu} + p$	50	130	236
$\nu_e + e^- \rightarrow \nu_e + e^-$	159	160	160
$\bar{\nu}_e + e^- \rightarrow \bar{\nu}_e + e^-$	65	66	67
$\nu_x + e^- \rightarrow \nu_x + e^-$	26	27	27
$\bar{\nu}_x + e^- \rightarrow \bar{\nu}_x + e^-$	23	23	23
$\nu_e + ^{12}\text{C} \rightarrow e^- + ^{12}\text{N}_{\text{g.s.}}$	44	114	214
$\bar{\nu}_e + ^{12}\text{C} \rightarrow e^+ + ^{12}\text{B}_{\text{g.s.}}$	49	107	177
$\nu + ^{12}\text{C} \rightarrow \nu' + ^{12}\text{C}^* \text{ (15.11)}$	26	60	104
$\bar{\nu} + ^{12}\text{C} \rightarrow \bar{\nu}' + ^{12}\text{C}^* \text{ (15.11)}$	24	56	95

rates [73, 74]. The background caused by the α decay of ^{210}Po in the energy range $0.2 - 0.5$ MeV can be reduced to manageable levels [75]. Most of the $\nu + p$ elastic scattering events are in the energy range $0.2 - 2$ MeV.

The differential rate of the number of neutrino interactions in the different detectable channels are calculated following the discussion in Ref. [11]. Table I shows the expected number of events in a liquid scintillator detector with a fiducial volume of 20 kton when different average energies of the neutrino flavors are assumed. From the table, it is clear that ν_e interactions on electrons are the largest in number among electron scattering interactions. The rate of $\nu + e^-$ scattering events has little dependence on the average energy of the neutrino spectrum. The steep energy dependence of the neutrino interactions on carbon is also evident from this table. These points imply that we will obtain the best constraint on the ν_e average energy by using the double coincidence signal of ν_e interaction on ^{12}C , whereas the electron scattering events will typically provide a better constraint on the total energy emitted in that particular flavor.

These signals can be divided into three broad categories depending on their temporal characteristics. The elastic scattering of neutrinos with electrons are a single-signal event in which the final state electron is detected. The neutral current scattering with the ^{12}C nuclei which produces the 15.11 MeV monochromatic gamma-ray photon is also a single-signal event. The inverse beta decay interaction is a double coincidence signal with a characteristic time of $200 \mu\text{s}$. The charged current interaction of ν_e and $\bar{\nu}_e$ on ^{12}C is also a double coincidence signal event in which the emitted charged leptons are separated by the time given by the half-life of the excited nucleus which is 11 or 20 msec.

D. Detection Strategy

We assume that the fiducial volume of the detector for supernova neutrino detection is 20 kton. The detector backgrounds are negligible above 0.2 MeV during a supernova burst. We closely follow the parameters of the detector that are described in [13] throughout this work.

It will be important to distinguish between the final states from $\nu_e + ^{12}\text{C}$ and $\bar{\nu}_e + ^{12}\text{C}$ interactions. Pulse shape distortion produced by positron can be used to distinguish between these interactions. The resultant nuclei in these interactions have a half-life of 11 msec and 20 msec, and this time structure can help to distinguish between these interactions. The slightly different end points of the positron and electron spectrum from $^{12}\text{N}_{\text{g.s.}}$ and $^{12}\text{B}_{\text{g.s.}}$ can also help. As the $\bar{\nu}_e$ spectrum will be known to $\sim 2\%$ precision from the inverse beta interaction, it can be used to predict the $\bar{\nu}_e + ^{12}\text{C}$ signal.

The left panel in Fig. 1 shows the recoil spectra for neutrino electron scattering events for ν_e . The electron scattering events due to $\bar{\nu}_e$ and ν_x are further suppressed and not shown for clarity (see Ref. [11]). We also show

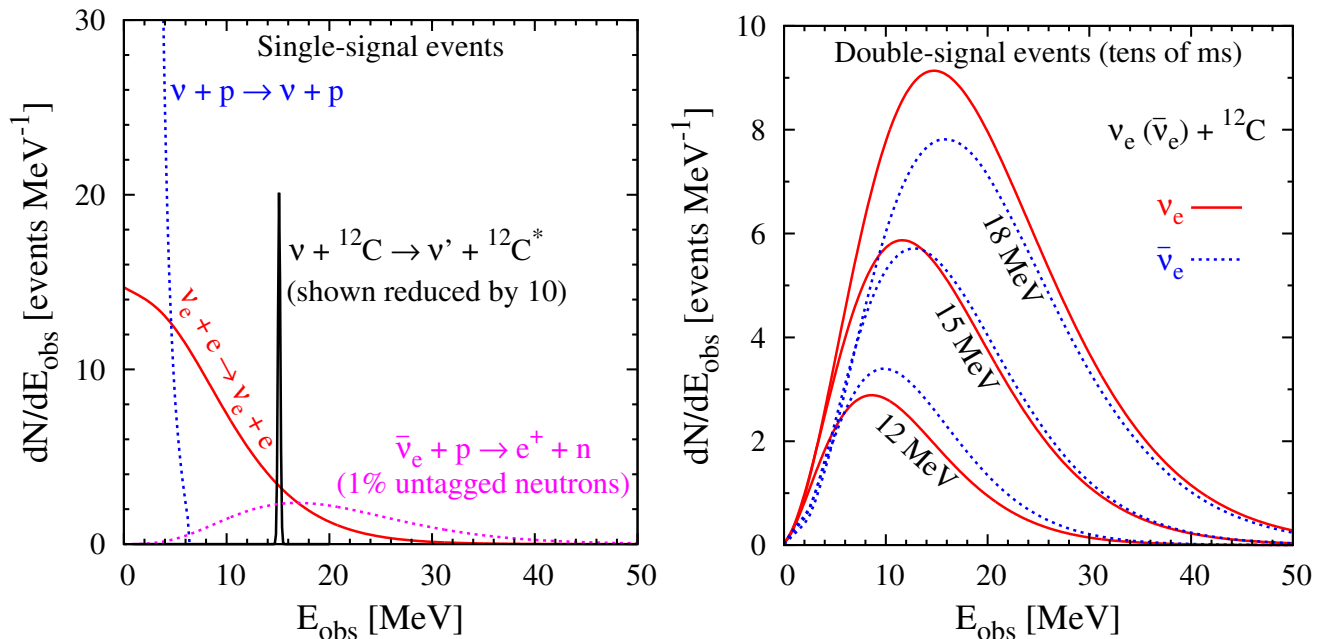


FIG. 1. Observed energy distribution in a 20 kton liquid scintillator detector for a Galactic supernova. In both panels, the total energy carried by each flavor of ν or $\bar{\nu}$ is 5×10^{52} erg. The ranges of the y-axes are different. **Left Panel:** We assume $\langle E_{\nu_e} \rangle = 12$ MeV, $\langle E_{\bar{\nu}_e} \rangle = 15$ MeV and $\langle E_{\nu_x} \rangle = 18$ MeV. We show the recoil spectrum of electrons in $\nu_e + e^-$ elastic scattering in solid red line. The total recoil spectrum of the protons in $\nu + p$ elastic scattering is shown by the dotted blue line. The recoil spectrum of the positron in the untagged inverse beta interaction is shown by the dotted magenta line, assuming 99% capture efficiency of neutrons. The monochromatic 15.11 MeV gamma-ray line due to $\nu + {}^{12}\text{C}$ neutral current interaction with $\langle E_{\nu} \rangle = 15.11$ MeV is shown in solid black line, including the effects of energy resolution [13] and reduced in height by a factor of 10. **Right panel:** We show the recoil spectrum of electrons and positrons from $\nu_e + {}^{12}\text{C}$ and $\bar{\nu}_e + {}^{12}\text{C}$ interactions. For both, the spectra are shown for three values of $\langle E_{\nu} \rangle$: 12 MeV, 15 MeV and 18 MeV. The electron and positron spectra are shown in solid red and dotted blue, respectively.

the differential event rate due to $\nu + p$ elastic scattering interactions, which is dominated by ν_x . We have taken the average energies of the various neutrino flavors as $\langle E_{\nu_e} \rangle = 12$ MeV, $\langle E_{\bar{\nu}_e} \rangle = 15$ MeV, and $\langle E_{\nu_x} \rangle = 18$ MeV in this plot. Other than neutrino-proton scattering, no other single-signal interactions can be reliably detected below 5 MeV.

In the right panel of Fig. 1, we plot the recoil spectra of the prompt charged lepton due to $\nu_e/\bar{\nu}_e + {}^{12}\text{C}$ charged current interactions. The resultant nuclei decay with known lifetimes. We show the recoil spectra of the resultant electron (positron) from the $\nu_e (\bar{\nu}_e) + {}^{12}\text{C}$ interaction for three values of the $\nu_e (\bar{\nu}_e)$ average energy, $\langle E \rangle = 12$ MeV, 15 MeV, and 18 MeV. The strong dependence of the average energy on these interactions is clearly visible in this plot.

III. CONSTRAINTS ON SUPERNOVA ν_e SPECTRAL PROPERTIES

In this section, we discuss the constraints on ν_e spectral parameters that can be obtained in a liquid scintillator detector. We will assume a range of average energies of the thermal ν_e spectrum to determine the impact of

neutrino oscillations in determining the ν_e spectral parameters. We will also show constraints for non-thermal ν_e spectrum.

A. Calculated Detection Spectra

Neutrino oscillations in a supernova occur via MSW mechanism and collective neutrino mixing. There is uncertainty in the neutrino spectrum before oscillation. Predicting the average energies of the neutrino spectrum after oscillation is difficult due to varying matter density inside the supernova. To take into account these uncertainties, we consider two extreme cases of ν_e average energy and total energy in terms of the underlying neutrino parameters and matter potential is complicated and can be done with least uncertainty after the occurrence of a Galactic supernova.

Case (A): $\langle E_{\nu_e} \rangle \approx 12$ MeV and $\langle E_{\nu_x} \rangle \approx 15 - 18$ MeV. In this case, there is no mixing between ν_e and ν_x and the hierarchy of average energies due to the late decoupling of ν_e is maintained.

Case (B): $\langle E_{\nu_e} \rangle \approx 15 - 18$ MeV, one flavor of ν_x has an average energy ≈ 12 MeV, and the other flavors of

ν_x have an average energy $\approx 15 - 18$ MeV. In this case, neutrino mixing has interchanged the average energy of ν_e and one of the ν_x . This case is easily distinguishable in a water Cherenkov detector with gadolinium due to the large number of $\nu_e + {}^{16}\text{O}$ scattering events [11].

Our initial aim is to constrain the ν_e spectral properties for case (A) and case (B). Spectral properties of all other neutrino flavors can be constrained by other neutrino interactions: inverse beta interactions will constrain the $\bar{\nu}_e$ spectral properties, and $\nu + p$ elastic scattering will constrain the ν_x spectral properties.

It is evident from Table I that the neutrino + ${}^{12}\text{C}$ charged current interactions are very sensitive to the average energy of the incoming neutrino spectrum. The strong energy dependence ensures that a strong constraint on the average energy of the neutrino spectrum will be deduced from this interaction. When the average energy of the neutrino spectrum is low, the number of neutrino + ${}^{12}\text{C}$ charged current interactions are low, and the constraint on the total energy carried by the neutrino flavor is weak. For higher values of $\langle E_{\nu_e} \rangle$, the constraints on the total energy carried by ν_e are stronger due to larger number of events.

The $\nu_e + {}^{12}\text{C}$ interactions can be detected with very high efficiency due to the double coincidence signal. There is a very small probability that a fully tagged inverse beta signal will coincide with the double coincidence signal of the $\nu_e + {}^{12}\text{C}$ interaction. The main reason for this is the factor ~ 50 difference in the characteristic time of the two double coincidence signatures (207 μsec v.s. 11 msec). The probability of a neutron capture on proton from inverse beta interaction to happen after 2 msec of the prompt positron signal is $\sim 6 \times 10^{-5}$.

The double coincidence signal of $\nu_e + {}^{12}\text{C}$ can be confused with the double coincidence signal of $\bar{\nu}_e + {}^{12}\text{C}$ unless the positrons are tagged efficiently. As mentioned earlier, positron detection via pulse shape distortion can be used to distinguish between these two interactions. Since present technology can only detect those positrons which annihilate after formation of ortho-positronium, about 55% of the $\bar{\nu}_e + {}^{12}\text{C}$ will pose a background to the signal from $\nu_e + {}^{12}\text{C}$ interaction. The factor ~ 2 difference in the decay times of the metastable nuclei can be further used to distinguish between these interactions. For conservativeness, we have assumed that all the $\bar{\nu}_e + {}^{12}\text{C}$ interactions will be a background to the $\nu_e + {}^{12}\text{C}$ signal. Detection of $\sim 45\%$ will help in a slight improvement of the constraints on total energy, whereas the improvement on average energy will be negligible. A future perfect discrimination of positrons from electrons can only improve this constraint at most by a factor of $\sim \sqrt{2}$.

B. Neutrino Spectral Parameter fit

We have performed the usual χ^2 analysis using a Poissonian likelihood function. [76]. We take the systematic

uncertainty on background and signal as 5% and 10% respectively. The short duration of a supernova burst means that the background is much less uncertain. The systematic uncertainty on the background and signal can only be properly quantified by the experimental collaboration. Due to $\sim 10\%$ uncertainties throughout the work, we use these values as indicative. We only fit for the ν_e spectral parameters as the spectral parameters of other flavors will be known from measurements in other detection channels.

We calculate the $\Delta\chi^2$ of the various best fit values. We use $\Delta\chi^2 = 4.6$ for two degrees of freedom to get the 90% C.L. regions. We have made various assumptions of the order of 10% throughout this work, so the contours should be understood with about 10% uncertainty.

Since the capture efficiency of neutrons on protons are unknown, we will show the contours for four different values of this efficiency: 90%, 95%, 99% and 100%. The contours obtained from $\nu_e + e^-$ scattering depend quite strongly on this capture efficiency. This is obvious as in the absence of neutron tagging, the prompt positrons from inverse beta interactions form a background to the search of recoil electrons from $\nu_e + e^-$ scattering.

The detection efficiency of neutrons have a negligible effect on the contours obtained from $\nu_e + {}^{12}\text{C}$ scattering. The double coincidence signal of $\nu_e + {}^{12}\text{C}$ interaction has a very different characteristic time compared to the inverse beta interaction. The inverse beta interactions with untagged neutrons are single-signal events and hence will not be confused with the double-signal event characteristic of $\nu_e + {}^{12}\text{C}$.

We show the likely constraints for case (A) in the left column of Fig. 2. The best fit parameters in this case are $\langle E_{\nu_e} \rangle = 12$ MeV and $E_{\nu_e}^{\text{tot}} = 5 \times 10^{52}$ erg and is shown by x. We show the contours for four different values of capture efficiency of neutrons : 90%, 95%, 99% and 100%. For this low value of $\langle E_{\nu_e} \rangle$, the constraint on the total energy from the $\nu_e + {}^{12}\text{C}$ charged current interaction is very weak. Due to the absence of directionality, the constraint from the $\nu_e + e^-$ elastic scattering is weaker than the constraint obtained from a water Cherenkov detector. The joint contour of the two detection channel is similar to that one can obtain by eye. The total energy carried by ν_e can be determined to $\sim 40\%$ precision and the average energy of ν_e can be determined to $\sim 25\%$ precision in this case.

When there is oscillation between ν_e and one of the flavors of ν_x , the constraints from $\nu_e + {}^{12}\text{C}$ charged current interactions become strong. These are shown in the right panel of Fig. 2. The best fit parameters shown by x are $\langle E_{\nu_e} \rangle = 18$ MeV and $E_{\nu_e}^{\text{tot}} = 5 \times 10^{52}$ erg. The increase in the average energy hardly increases the number of events from $\nu_e + e^-$ elastic scattering and hence the constraints on average energies from this elastic scattering is extremely weak. The large number of $\nu_e + {}^{12}\text{C}$ charged current interactions ensure that the constraints obtained from the double coincidence signal is extremely strong. In this case, the total energy carried by ν_e is de-

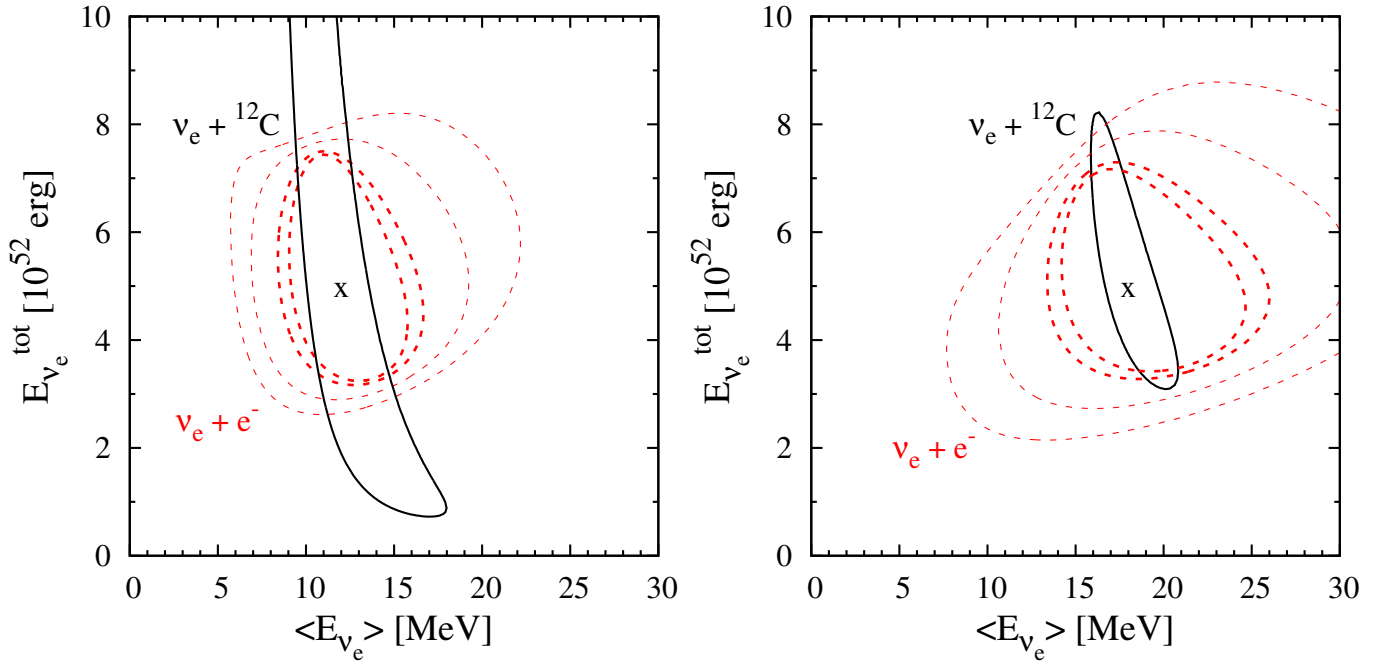


FIG. 2. Allowed parameter space (90% C.L. $\Delta\chi^2$ contours) for the ν_e spectrum parameters using the $\nu_e + e^-$ and $\nu_e + ^{12}\text{C}$ channels. We do not show the combined constraints which closely follow as would be expected visually. The best fit point in both the panels are shown by x. The total energy carried by all the neutrino flavors is 5×10^{52} erg. In both cases we have closed contours on the neutrino spectral properties. The four contours for the $\nu_e + e^-$ scattering events are for a neutron detection efficiency of 90%, 95%, 99% and 100% with decreasing distance from the point marked x respectively. The capture efficiency of neutrons on proton will not have a large impact on the contour obtained from the $\nu_e + ^{12}\text{C}$ interaction. **Left Panel:** $\langle E_{\nu_e} \rangle = 12$ MeV and $\langle E_{\nu_x} \rangle = 18$ MeV. **Right Panel:** $\langle E_{\nu_e} \rangle = 18$ MeV, i.e., one of the ν_x has oscillated into ν_e .

terminated to $\sim 40\%$ precision and the average energy is determined to $\sim 10\%$ precision.

As is easily seen from the figure, the sharp energy dependence of the $\nu_e + ^{12}\text{C}$ interaction will help separate the two cases when the average neutrino energies are far apart. This is an important result and it will help us understand supernova much better. Both the $\nu_e + e^-$ scattering and the $\nu_e + ^{12}\text{C}$ scattering give weak constraints on the total energy carried by the ν_e flavor.

For the joint contours, the stronger constraint on the $\langle E_{\nu_e} \rangle$ is always obtained from the $\nu_e + ^{12}\text{C}$ interaction. The stronger constraint on the $E_{\nu_e}^{\text{tot}}$ is generally obtained from the $\nu_e + e^-$ interaction, unless the $\langle E_{\nu_e} \rangle$ is high such that there are a large number of $\nu_e + ^{12}\text{C}$ interactions. This complementary information carried by both the interactions should be fully utilized to obtain the best information from these two important channels for ν_e detection in liquid scintillator detector.

The part of the neutrino spectrum probed by $\nu_e + e^-$ elastic scattering and $\nu_e + ^{12}\text{C}$ charged current interaction is quite different and is shown in Fig. 3. The detection threshold is taken to be 5 MeV, and hence the part of the neutrino spectrum probed by $\nu_e + e^-$ and $\nu_e + ^{12}\text{C}$ charged current interaction is $\gtrsim 5.2$ MeV and $\gtrsim 22.5$ MeV respectively. The $\nu_e + ^{12}\text{C}$ charged current interaction is only sensitive to higher neutrino energies, and hence the strong dependence on the neutrino average

energy. A slight change in the neutrino average energy will change the tail of the spectrum significantly and this explains the strong constraint on $\langle E_{\nu_e} \rangle$ obtained from the $\nu_e + ^{12}\text{C}$ interaction.

We now discuss cases in which the average energy of the incoming ν_e spectrum have less hierarchy. Modern computer simulations of supernova explosion typically show a much closer range of the average energy of neutrinos of different flavors [77], $\langle E_{\nu_e} \rangle \approx 11$ MeV, and $\langle E_{\bar{\nu}_e} \rangle \approx \langle E_{\nu_x} \rangle \approx 14$ MeV. In our companion paper [11], we had taken these values to be 11 MeV and 15 MeV. The potential better discrimination possible in a large liquid scintillator detector motivates us to consider this slightly more challenging situation. Due to the proximity of the average energies, it is much more difficult to determine whether $\nu_e \leftrightarrow \nu_x$ oscillations have taken place.

We show the 90% joint contours (using both the neutrino electron elastic scattering and neutrino carbon charged current interaction) for this situation in Fig. 4. The efficiency of neutron detection is taken to be 100% in this plot. The total energy carried by each neutrino flavor is taken to be 5×10^{52} erg. The strong energy dependence of the neutrino carbon charged current interactions help us separate the two cases of mildly differing average energies. This will be an important physics motivation for large liquid scintillator detectors. The height of both these contours depend on the constraint from ν_e

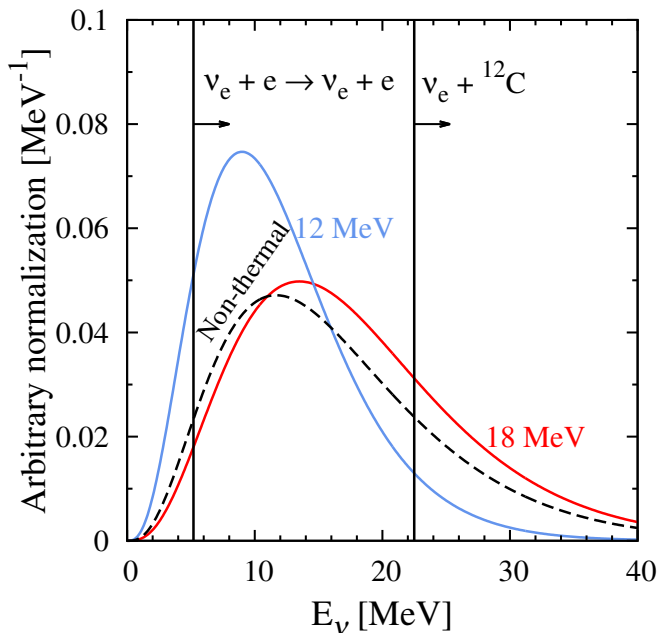


FIG. 3. The neutrino spectrum from a supernova and the part of the spectrum probed by $\nu_e + e^-$ elastic scattering and $\nu_e + {}^{12}\text{C}$ charged current interaction. The neutrino spectrum (Eqn. 1) is shown for two different average energies of 12 MeV and 18 MeV in blue and red respectively. The part of the neutrino spectrum probed by $\nu_e + e^-$ spectrum (> 5.2 MeV) and by $\nu_e + {}^{12}\text{C}$ charged current interaction (> 22.5 MeV) is shown by vertical lines. We also show a non-thermal spectrum in dashed black which results from MSW mixing in the inverted hierarchy due to the two thermal spectra shown in the figure.

+ e^- scattering and the $\nu_e + {}^{12}\text{C}$ charged current scattering controls the width of these contours. Having a less than perfect capture efficiency of neutrons will degrade this constraint on the total energy but will not affect the separation in the average energies.

C. Non-thermal ν_e spectrum

As a final illustration of the discriminating power of large liquid scintillator detectors, we try to reconstruct the spectral parameters for a non-thermal spectrum of incoming ν_e . We only consider MSW oscillations for this example [3, 78]. Collective oscillations will generally complicate the situation further and a dedicated study is required for that purpose [5, 79]. The normal hierarchy scenario in MSW mixing is similar to the ones we considered earlier in this work: the final ν_e spectrum emitted from the supernova is the initial ν_x spectrum.

In the inverted hierarchy for MSW mixing, the final ν_e spectrum is a mixture of the initial ν_e spectrum (mixing probability = $\sin^2 \theta_\odot$) and the initial ν_x spectrum (mixing probability = $1 - \sin^2 \theta_\odot$). If the original ν_e and ν_x average energy is 12 MeV and 18 MeV respectively, then

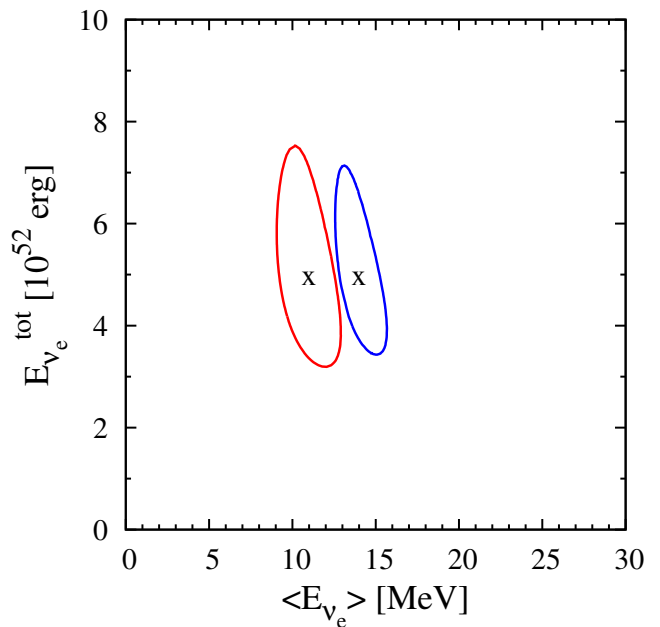


FIG. 4. Joint 90% C.L. $\Delta\chi^2$ contours for ν_e spectrum parameters determined from the $\nu_e + e^-$ and $\nu_e + {}^{12}\text{C}$ channels. We distinguish two different cases of ν_e average energies here, 11 MeV and 14 MeV. The total energy carried by the neutrino flavor is 5×10^{52} erg.

the final spectrum after MSW mixing is shown by the black dashed curve in Fig. 3.

The total spectrum is then determined by 4 parameters: the total and average energy carried by the ν_e and ν_x flavor. We can relate the total energies carried by ν_e and ν_x flavor since we will know the total binding energy of the supernova and the total energy carried by $\bar{\nu}_e$ (from inverse beta interactions). This reduces the number of free parameters to three.

Due to the non-thermal spectrum and the three free parameters, a complete scan of the parameter space is complicated and require a dedicated study. We will show the allowed contours for the initial average energies carried by the ν_e ($\langle E_{\nu_e} \rangle^0$) and ν_x ($\langle E_{\nu_x} \rangle^0$) flavor assuming that the total energy carried by the neutrino flavors is 5×10^{52} erg. For a full scan, we have to vary the value of the total energy carried by the neutrino flavors. We fix it to a fiducial value here for a simple pedagogical example.

Since the spectrum has a non-linear dependence on the average energies, we only show the constraints on $\langle E_{\nu_e} \rangle^0$ and $\langle E_{\nu_x} \rangle^0$ in Fig. 5. The best fit point, shown by x, is given by $\langle E_{\nu_e} \rangle^0 = 12$ MeV and $\langle E_{\nu_x} \rangle^0 = 18$ MeV. The rectangle encloses the range $10 \text{ MeV} \leq \langle E_{\nu_e} \rangle^0 \leq 15 \text{ MeV}$, and $10 \text{ MeV} \leq \langle E_{\nu_x} \rangle^0 \leq 20 \text{ MeV}$, which is approximately the theoretically favored region according to supernova simulations. The lower part of the rectangle shaded in red is disfavored as we expect $\langle E_{\nu_x} \rangle^0 > \langle E_{\nu_e} \rangle^0$.

We show the constraint from both $\nu_e + {}^{12}\text{C}$ and $\nu_e + {}^{16}\text{O}$ interaction in a near-future large liquid scintillator detector and gadolinium loaded Super-Kamiokande

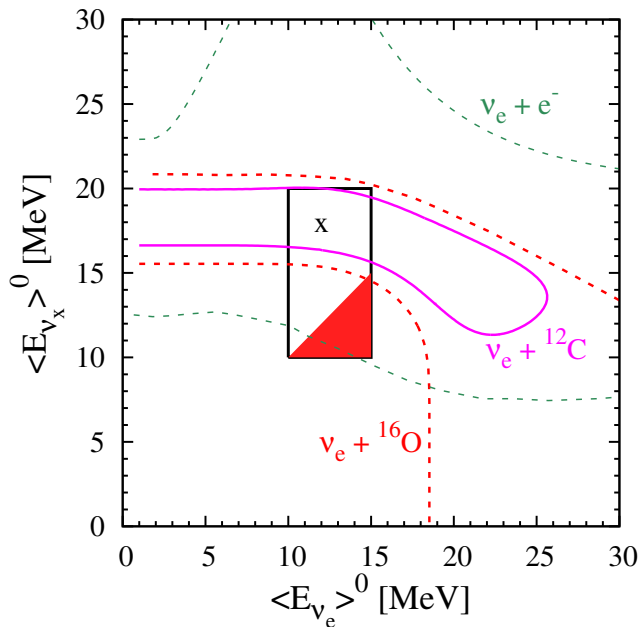


FIG. 5. 90% C.L. $\Delta\chi^2$ contours for a non-thermal spectrum of ν_e in the plane of initial ν_e and ν_x average energies. We take the example of MSW mixing in inverted hierarchy — the incoming ν_e spectrum is given by an appropriate mixture of ν_e and ν_x spectrum (see black dashed curve in Fig. 3). We fix the total energy carried by the ν_e and ν_x flavor as 5×10^{52} erg. The best fit point for the initial average energies for ν_e and ν_x is given by x. The contour obtained from the $\nu_e + {}^{16}\text{O}$ and $\nu_e + {}^{12}\text{C}$ interaction in gadolinium loaded Super-Kamiokande and future large liquid scintillator detector is given by the red dashed line and magenta line respectively. The constraint obtained from $\nu_e + e^-$ scattering in a gadolinium loaded Super-Kamiokande detector is shown in dashed green. We have assumed a neutron capture efficiency of 90% in gadolinium loaded Super-Kamiokande to obtain this result. The rectangle shows the theoretically expected region of $\langle E_{\nu_e} \rangle^0$ and $\langle E_{\nu_x} \rangle^0$. The lower part of the rectangle shaded in red is excluded since $\langle E_{\nu_e} \rangle^0 > \langle E_{\nu_x} \rangle^0$ in that region, which is contrary to theoretical expectations.

respectively. We also show the constraint from $\nu_e + e^-$ interactions in gadolinium loaded Super-Kamiokande detector. We assume that the neutron capture efficiency on gadolinium in Super-Kamiokande and on protons (and carbon) in liquid scintillator detector is 90% and 100% respectively. As is evident from the black dashed curve in Fig. 3, the non-thermal spectrum at high energies is mostly due to the flavor with higher average energy. This explains the nearly horizontal behavior of the contours for the neutrino nucleus interactions. The constraint on the flavor with higher average energy is around 10% and which is approximately equal to the constraint that one can achieve from $\nu + p$ interaction as well. The $\nu_e + e^-$ elastic scattering is nearly independent of the average energy and hence the constraint from that interaction is very broad and uninformative.

The constraint obtained from the $\nu_e + {}^{16}\text{O}$ interac-

tion in gadolinium loaded Super-Kamiokande is slightly weaker due to the larger number of background events. In this plot, a contour with a smaller area denotes better discriminating power. The constrained area is approximately 46% of the theoretically favored region. Lowering the threshold of the neutrino nucleus interaction will further improve these constraints. Our results should encourage the experimentalists to optimise their cuts to detect $\nu_e + {}^{12}\text{C}$ interaction in a very efficient manner, since this interaction will give us the strongest constraint on the average energies for a non-thermal spectrum.

We can compare the results obtained in the supernova ν_e detection in Super-Kamiokande loaded with gadolinium [11] with the results obtained in this work. It is important to detect supernova neutrinos in many different detectors as earth matter effects can be understood if the detectors are far apart. Detection of neutrinos in two different detection methods will also improve the reliability of the detection. The presence of directionality in water Cherenkov detectors help in finding the direction of the Galactic supernova; this is not possible in a liquid scintillator detector. The charged current neutrino interaction on ${}^{16}\text{O}$ is more uncertain than the corresponding interaction on ${}^{12}\text{C}$ as the latter has been measured. One advantage for water Cherenkov detectors is that they can be designed to be a factor of ~ 20 larger than Super-Kamiokande with the current technology and there is active research in that direction [80]. Having such a large water Cherenkov detector loaded with gadolinium will improve the uncertainties of the ν_e spectral parameters by a factor of ~ 5 [11]. Currently there are no plans to build a liquid scintillator detector of the size of Hyper-Kamiokande. Detection of supernova ν_e in these two different detectors will involve different systematics and this will help in improving our knowledge of supernova physics.

IV. CONCLUSIONS

Detecting supernova neutrinos is important for astrophysics and neutrino physics [81–98]. In spite of detecting numerous supernovae via electromagnetic signal, we still do not completely understand a supernova. One of the main reasons behind this is that the total energy budget of the supernova is completely dominated by neutrinos. The only way to completely understand a supernova is to detect all flavors of neutrinos emitted by it. No one type of detection technique is completely efficient in detecting all the supernova neutrino flavors and hence it is essential to look into various different detector types to improve our knowledge of supernova neutrinos. It is important to detect supernova neutrinos in different detectors to increase detectability of the signal as other detectors might not be working during that short period of time.

Detection of supernova ν_e in a gadolinium loaded water Cherenkov detector was investigated in [11]. In this

companion work, we determine the feasibility of detecting supernova ν_e in near-future large liquid scintillator detector. The detection technique in these two different detectors are different and we gain more knowledge in detecting supernova ν_e in both these different types of detectors. The main interactions of ν_e in a liquid scintillator detector are its elastic scattering with electrons and charged current interaction with ^{12}C nuclei. The former interaction is almost independent of the average energy of the ν_e flavor, but the later interaction will give us a precise measure of the average energy of the ν_e .

As in any supernova neutrino detection technique, the largest background for the ν_e detection is the inverse beta interaction caused by the supernova $\bar{\nu}_e$. Neutron capture on proton and carbon will help reduce this enormous background. The charged current interaction of ν_e on ^{12}C nuclei can be distinguished by the double coincidence signal of this interaction. There is a possibility that this interaction might be confused with charged current interaction of $\bar{\nu}_e$ with ^{12}C ; identification of positron via pulse shape distortion and the separation of the events due to the different decay times of the metastable nuclei will help in their distinction. It should also be possible to statistically subtract the $\bar{\nu}_e$ charged current interaction as inverse beta interactions will give us a very precise measure of the $\bar{\nu}_e$ spectrum. The neutral current interaction of neutrinos on ^{12}C will also help in deterring the total binding energy of the supernova independent of oscillation physics.

The main results of this work is shown in Figs. 2, 4 and 5. From Fig. 2, we find that the total energy and the average energy carried by the ν_e flavor will be known to $\lesssim 25\%$ and 40% precision respectively. More importantly, 20 kton liquid scintillator detectors can distinguish between whether the average energy of ν_e is 11 MeV or 14 MeV (Fig. 4). This ability to distinguish between differ-

ent ν_e average energies make liquid scintillator detector an important tool in understanding supernova. The interesting constraint on the initial average energies of the ν_e and ν_x flavors for a non-thermal spectrum of ν_e due to MSW mixing in inverted hierarchy is shown in Fig. 5.

All the constraints presented in this work can potentially be improved by a factor of $\sim \sqrt{2}$ if data from two independent and similar sized detectors like JUNO and RENO-50 are combined. If a larger detector like LENA detects supernova neutrinos, then LENA by itself should improve the presented constraints by a factor of ~ 1.6 . Supernova ν_e can be detected with high precision in large liquid Argon detectors which are not yet built [99, 100].

It is interesting to note that a liquid scintillator detector can detect all the different flavors of supernova neutrinos: $\bar{\nu}_e$ through inverse beta interaction, ν_x through the elastic scattering with protons and ν_e through its elastic interaction with electrons and charged current interaction with ^{12}C . Due to the serious interest in large liquid scintillator detectors [13, 15, 60, 64, 65], it is important for people to look into the details of supernova neutrino detection in these detectors. We hope that our work will encourage the experimentalists to optimize their cuts to detect the neutrino signal from a Galactic supernova.

ACKNOWLEDGMENTS

We thank Basudeb Dasgupta, Shunsaku Horiuchi, Patrick Huber, Leonidas Kalousis, Matthew Kistler, Jonathan Link, Shirley Li, Camillo Mariani and Yifang Wang for discussions. RL was supported in the initial part of the work by NSF Grant PHY-1101216 awarded to JFB. JFB was supported by NSF Grant PHY-1101216 and PHY-1404311. S.K.A. acknowledges the support from DST/INSPIRE Research Grant [IFA-PH-12], Department of Science and Technology, India.

-
- [1] B. Mueller and H. T. Janka, “Non-Radial Instabilities and Progenitor Asphericities in Core-Collapse Supernovae”, [arXiv:1409.4783](#).
 - [2] A. Wongwathanarat, E. Mueller, and H.-T. Janka, “Three-Dimensional Simulations of Core-Collapse Supernovae: From Shock Revival to Shock Breakout”, [arXiv:1409.5431](#).
 - [3] A. S. Dighe and A. Y. Smirnov, “Identifying the neutrino mass spectrum from the neutrino burst from a supernova”, *Phys. Rev.* **D62** (2000) 033007, [arXiv:hep-ph/9907423](#).
 - [4] H. Duan, G. M. Fuller, and Y.-Z. Qian, “Collective Neutrino Oscillations”, *Ann.Rev.Nucl.Part.Sci.* **60** (2010) 569–594, [arXiv:1001.2799](#).
 - [5] B. Dasgupta, “Physics and Astrophysics Opportunities with Supernova Neutrinos”, *POS ICHEP2010* (2010) 294, [arXiv:1005.2681](#).
 - [6] P. Vogel and J. F. Beacom, “Angular distribution of neutron inverse beta decay”, *Phys.Rev.* **D60** (1999) 053003, [arXiv:hep-ph/9903554](#).
 - [7] A. Strumia and F. Vissani, “Precise quasielastic neutrino/nucleon cross-section”, *Phys.Lett.* **B564** (2003) 42–54, [arXiv:astro-ph/0302055](#).
 - [8] **IceCube** Collaboration, R. Abbasi *et al.*, “IceCube Sensitivity for Low-Energy Neutrinos from Nearby Supernovae”, *Astron.Astrophys.* **535** (2011) A109, [arXiv:1108.0171](#).
 - [9] J. F. Beacom, W. M. Farr, and P. Vogel, “Detection of supernova neutrinos by neutrino proton elastic scattering”, *Phys.Rev.* **D66** (2002) 033001, [arXiv:hep-ph/0205220](#).
 - [10] B. Dasgupta and J. F. Beacom, “Reconstruction of supernova ν_μ , ν_τ , anti- ν_μ , and anti- ν_τ neutrino spectra at scintillator detectors”, *Phys.Rev.* **D83** (2011) 113006, [arXiv:1103.2768](#).

- [11] R. Laha and J. F. Beacom, “Gadolinium in water Cherenkov detectors improves detection of supernova ν_e ”, *Phys.Rev.* **D89** (2014) 063007, [arXiv:1311.6407](#).
- [12] **JUNO** Collaboration, M. He, “Jiangmen Underground Neutrino Observatory”, [arXiv:1412.4195](#).
- [13] Y.-F. Li, “Overview of the Jiangmen Underground Neutrino Observatory (JUNO)”, *International Journal of Modern Physics: Conference Series*, 2014 [arXiv:1402.6143](#).
- [14] S.-B. Kim, “New results from RENO and prospects with RENO-50”, [arXiv:1412.2199](#).
- [15] **LENA** Collaboration, M. Wurm *et al.*, “The next-generation liquid-scintillator neutrino observatory LENA”, *Astropart.Phys.* **35** (2012) 685–732, [arXiv:1104.5620](#).
- [16] S. M. Adams, C. Kochanek, J. F. Beacom, M. R. Vagins, and K. Stanek, “Observing the Next Galactic Supernova”, [arXiv:1306.0559](#).
- [17] M. T. Keil, G. G. Raffelt, and H.-T. Janka, “Monte Carlo study of supernova neutrino spectra formation”, *Astrophys.J.* **590** (2003) 971–991, [arXiv:astro-ph/0208035](#).
- [18] I. Tamborra, B. Muller, L. Hudepohl, H.-T. Janka, and G. Raffelt, “High-resolution supernova neutrino spectra represented by a simple fit”, *Phys.Rev.* **D86** (2012) 125031, [arXiv:1211.3920](#).
- [19] B. Dasgupta and A. Dighe, “Collective three-flavor oscillations of supernova neutrinos”, *Phys.Rev.* **D77** (2008) 113002, [arXiv:0712.3798](#).
- [20] B. Dasgupta, A. Dighe, A. Mirizzi, and G. G. Raffelt, “Spectral split in prompt supernova neutrino burst: Analytic three-flavor treatment”, *Phys.Rev.* **D77** (2008) 113007, [arXiv:0801.1660](#).
- [21] A. Dighe, “Physics potential of future supernova neutrino observations”, *J.Phys.Conf.Ser.* **136** (2008) 022041, [arXiv:0809.2977](#).
- [22] B. Dasgupta, A. Dighe, G. G. Raffelt, and A. Y. Smirnov, “Multiple Spectral Splits of Supernova Neutrinos”, *Phys.Rev.Lett.* **103** (2009) 051105, [arXiv:0904.3542](#).
- [23] B. Dasgupta, G. G. Raffelt, and I. Tamborra, “Triggering collective oscillations by three-flavor effects”, *Phys.Rev.* **D81** (2010) 073004, [arXiv:1001.5396](#).
- [24] B. Dasgupta, A. Mirizzi, I. Tamborra, and R. Tomas, “Neutrino mass hierarchy and three-flavor spectral splits of supernova neutrinos”, *Phys.Rev.* **D81** (2010) 093008, [arXiv:1002.2943](#).
- [25] H. Duan, A. Friedland, G. C. McLaughlin, and R. Surman, “The influence of collective neutrino oscillations on a supernova r-process”, *J.Phys.* **G38** (2011) 035201, [arXiv:1012.0532](#).
- [26] A. Friedland, “Self-refraction of supernova neutrinos: mixed spectra and three-flavor instabilities”, *Phys.Rev.Lett.* **104** (2010) 191102, [arXiv:1001.0996](#).
- [27] Y. Pehlivan, A. Balantekin, T. Kajino, and T. Yoshida, “Invariants of Collective Neutrino Oscillations”, *Phys.Rev.* **D84** (2011) 065008, [arXiv:1105.1182](#).
- [28] S. Sarikas, G. G. Raffelt, L. Hudepohl, and H.-T. Janka, “Suppression of Self-Induced Flavor Conversion in the Supernova Accretion Phase”, *Phys.Rev.Lett.* **108** (2012) 061101, [arXiv:1109.3601](#).
- [29] J. F. Cherry, J. Carlson, A. Friedland, G. M. Fuller, and A. Vlasenko, “Neutrino scattering and flavor transformation in supernovae”, *Phys.Rev.Lett.* **108** (2012) 261104, [arXiv:1203.1607](#).
- [30] E. Borriello, S. Chakraborty, H.-T. Janka, E. Lisi, and A. Mirizzi, “Turbulence patterns and neutrino flavor transitions in high-resolution supernova models”, [arXiv:1310.7488](#).
- [31] S. Chakraborty, A. Mirizzi, N. Saviano, and D. d. S. Seixas, “Suppression of the multi-azimuthal-angle instability in dense neutrino gas during supernova accretion phase”, [arXiv:1402.1767](#).
- [32] C. Lunardini and A. Y. Smirnov, “Supernova neutrinos: Earth matter effects and neutrino mass spectrum”, *Nucl.Phys.* **B616** (2001) 307–348, [arXiv:hep-ph/0106149](#).
- [33] A. S. Dighe, M. T. Keil, and G. G. Raffelt, “Identifying earth matter effects on supernova neutrinos at a single detector”, *JCAP* **0306** (2003) 006, [arXiv:hep-ph/0304150](#).
- [34] A. Dighe, M. Kachelriess, G. Raffelt, and R. Tomas, “Signatures of supernova neutrino oscillations in the earth mantle and core”, *JCAP* **0401** (2004) 004, [arXiv:hep-ph/0311172](#).
- [35] E. Borriello, S. Chakraborty, A. Mirizzi, P. D. Serpico, and I. Tamborra, “(Down-to-)Earth matter effect in supernova neutrinos”, *Phys.Rev.* **D86** (2012) 083004, [arXiv:1207.5049](#).
- [36] L. Cadonati, F. Calaprice, and M. Chen, “Supernova neutrino detection in borexino”, *Astropart.Phys.* **16** (2002) 361–372, [arXiv:hep-ph/0012082](#).
- [37] P. Machado, T. Muhlbeier, H. Nunokawa, and R. Zukanovich Funchal, “Potential of a Neutrino Detector in the ANDES Underground Laboratory for Geophysics and Astrophysics of Neutrinos”, *Phys.Rev.* **D86** (2012) 125001, [arXiv:1207.5454](#).
- [38] K. Scholberg, “Supernova Neutrino Detection”, *Ann.Rev.Nucl.Part.Sci.* **62** (2012) 81–103, [arXiv:1205.6003](#).
- [39] C. Lujan-Peschard, G. Pagliaroli, and F. Vissani, “Spectrum of Supernova Neutrinos in Ultra-pure Scintillators”, [arXiv:1402.6953](#).
- [40] **KamLAND** Collaboration, K. Tllich, “Supernova detection with KamLAND”, *Nucl.Phys.Proc.Suppl.* **221** (2011) 355.
- [41] **Double Chooz** Collaboration, Y. Abe *et al.*, “First Measurement of θ_{13} from Delayed Neutron Capture on Hydrogen in the Double Chooz Experiment”, *Phys.Lett.* **B723** (2013) 66–70, [arXiv:1301.2948](#).
- [42] **Daya Bay** Collaboration, F. An *et al.*, “Independent Measurement of θ_{13} via Neutron Capture on Hydrogen at Daya Bay”, [arXiv:1406.6468](#).
- [43] **RENO** Collaboration, “New results from RENO”, <http://neutrino2014.bu.edu/>, 2014.
- [44] J. F. Beacom and M. R. Vagins, “GADZOOKS! Anti-neutrino spectroscopy with large water Cherenkov detectors”, *Phys.Rev.Lett.* **93** (2004) 171101, [arXiv:hep-ph/0309300](#).

- [45] B. von Krosigk, L. Neumann, R. Nolte, S. Rottger, and K. Zuber, “Measurement of the proton light response of various LAB based scintillators and its implication for supernova neutrino detection via neutrino-proton scattering”, *Eur.Phys.J.* **C73** (2013) 2390, [arXiv:1301.6403](#).
- [46] M. Fukugita, Y. Kohyama, and K. Kubodera, “Neutrino reaction cross-sections on C-12 target”, *Phys.Lett.* **B212** (1988) 139.
- [47] E. Kolbe, F. Thielemann, K. Langanke, and P. Vogel, “Inclusive C-12($\nu/\mu, \mu$)N-12 reaction in the continuum random phase approximation”, *Phys.Rev.* **C52** (1995) 3437–3441.
- [48] J. Engel, E. Kolbe, K. Langanke, and P. Vogel, “Neutrino induced transitions between the ground states of the A=12 triad”, *Phys.Rev.* **C54** (1996) 2740–2744, [arXiv:nucl-th/9606031](#).
- [49] E. Kolbe, K. Langanke, and P. Vogel, “Weak reactions on C-12 within the continuum random phase approximation with partial occupancies”, *Nucl.Phys.* **A652** (1999) 91–100, [arXiv:nucl-th/9903022](#).
- [50] A. Hayes and I. Towner, “Shell model calculations of neutrino scattering from C-12”, *Phys.Rev.* **C61** (2000) 044603, [arXiv:nucl-th/9907049](#).
- [51] C. Volpe, N. Auerbach, G. Colo, T. Suzuki, and N. Van Giai, “Microscopic theories of neutrino C-12 reactions”, *Phys.Rev.* **C62** (2000) 015501, [arXiv:nucl-th/0001050](#).
- [52] **LSND** Collaboration, L. Auerbach *et al.*, “Measurements of charged current reactions of $\nu(e)$ on ^{12}C ”, *Phys.Rev.* **C64** (2001) 065501, [arXiv:hep-ex/0105068](#).
- [53] Y. Kino *et al.*, “Positron Annihilation in Liquid Scintillator for Electron Antineutrino Detection”, *J. Nucl. Radiochem. Sci.* **1** (2000) 63.
- [54] D. Franco, G. Consolati, and D. Trezzi, “Positronium signature in organic liquid scintillators for neutrino experiments”, *Phys. Rev. C* **83** (2011), no. 1, 015504, [arXiv:1011.5736](#).
- [55] **Borexino** Collaboration, G. Bellini *et al.*, “Final results of Borexino Phase-I on low energy solar neutrino spectroscopy”, [arXiv:1308.0443](#).
- [56] Y. Abe, J. dos Anjos, J. Barriere, E. Baussan, I. Bekman, *et al.*, “Ortho-positronium observation in the Double Chooz Experiment”, *JHEP* **1410** (2014) 32, [arXiv:1407.6913](#).
- [57] T. Yoshida, T. Suzuki, S. Chiba, T. Kajino, H. Yokomakura, *et al.*, “Neutrino-Nucleus Reaction Cross Sections for Light Element Synthesis in Supernova Explosions”, *Astrophys.J.* **686** (2008) 448–466, [arXiv:0807.2723](#).
- [58] A. Ianni, D. Montanino, and F. Villante, “How to observe B-8 solar neutrinos in liquid scintillator detectors”, *Phys.Lett.* **B627** (2005) 38–48, [arXiv:physics/0506171](#).
- [59] T. Suzuki, A. Balantekin, and T. Kajino, “Neutrino Capture on ^{13}C ”, *Phys.Rev.* **C86** (2012) 015502, [arXiv:1204.4231](#).
- [60] K. N. R. Center, “International Workshop on ”RENO-50” toward Neutrino Mass Hierarchy”, <http://home.kias.re.kr/MKG/h/reno50/?pageNo=114>, 2013.
- [61] P. Bakhti and Y. Farzan, “Constraining Super-light Sterile Neutrino Scenario by JUNO and RENO-50”, *JHEP* **1310** (2013) 200, [arXiv:1308.2823](#).
- [62] P. Bakhti and Y. Farzan, “Shedding light on LMA-Dark solar neutrino solution by medium baseline reactor experiments: JUNO and RENO-50”, *JHEP* **1407** (2014) 064, [arXiv:1403.0744](#).
- [63] J. Park, “Study of Neutrino Mass Hierarchy with RENO-50”, *PoS Neutel2013* (2013) 076.
- [64] R. Mllenberg, F. von Feilitzsch, D. Hellgartner, L. Oberauer, M. Tippmann, *et al.*, “Detecting the Diffuse Supernova Neutrino Background with LENA”, [arXiv:1409.2240](#).
- [65] R. Mllenberg, F. von Feilitzsch, D. Hellgartner, L. Oberauer, M. Tippmann, *et al.*, “Detecting the Upturn of the Solar ^8B Neutrino Spectrum with LENA”, *Phys.Lett.* **B737** (2014) 251–255, [arXiv:1408.0623](#).
- [66] A. Gando, Y. Gando, K. Ichimura, H. Ikeda, K. Inoue, *et al.*, “A study of extraterrestrial antineutrino sources with the KamLAND detector”, *Astrophys.J.* **745** (2012) 193, [arXiv:1105.3516](#).
- [67] **Borexino** Collaboration, G. Bellini *et al.*, “Cosmogenic Backgrounds in Borexino at 3800 m water-equivalent depth”, *JCAP* **1308** (2013) 049, [arXiv:1304.7381](#).
- [68] J. A. Detwiler, “Measurement of neutrino oscillation with KamLAND”, 2005.
- [69] D. A. Dwyer, “Precision Measurement of Neutrino Oscillation Parameters with KamLAND”, 2007.
- [70] **KamLAND** Collaboration, S. Abe *et al.*, “Precision Measurement of Neutrino Oscillation Parameters with KamLAND”, *Phys.Rev.Lett.* **100** (2008) 221803, [arXiv:0801.4589](#).
- [71] V. Kudryavtsev, N. Spooner, and J. McMillan, “Simulations of muon induced neutron flux at large depths underground”, *Nucl.Instrum.Meth.* **A505** (2003) 688–698, [arXiv:hep-ex/0303007](#).
- [72] H. Arslan and M. Bektasoglu, “Geant4 Simulation Study of Deep Underground Muons: Vertical Intensity and Angular Distribution”, *Adv.High Energy Phys.* **2013** (2013) 391573.
- [73] **Borexino** Collaboration, G. Bellini *et al.*, “New experimental limits on the Pauli forbidden transitions in C-12 nuclei obtained with 485 days Borexino data”, *Phys.Rev.* **C81** (2010) 034317, [arXiv:0911.0548](#).
- [74] **Borexino** Collaboration, G. Bellini *et al.*, “Neutrinos from the primary proton - proton fusion process in the Sun”, *Nature* **512** (2014), no. 7515, 383–386.
- [75] F. Villante, A. Ianni, F. Lombardi, G. Pagliaroli, and F. Vissani, “A Step toward CNO solar neutrinos detection in liquid scintillators”, *Phys.Lett.* **B701** (2011) 336–341, [arXiv:1104.1335](#).
- [76] S. K. Agarwalla, S. Choubey, and A. Raychaudhuri, “Neutrino mass hierarchy and θ_{13} with a magic baseline beta-beam experiment”, *Nucl.Phys.* **B771** (2007) 1–27, [arXiv:hep-ph/0610333](#).
- [77] B. Mueller, H.-T. Janka, and A. Heger, “New Two-Dimensional Models of Supernova Explosions by the Neutrino-Heating Mechanism: Evidence for Different Instability Regimes in Collapsing Stellar Cores”, *Astrophys.J.* **761** (2012) 72, [arXiv:1205.7078](#).
- [78] A. Dighe, “Neutrinos from a core collapse supernova”, *AIP Conf. Proc.* **981** (2008) 75 – 79, [arXiv:0712.4386](#).

- [79] S. Choubey, B. Dasgupta, A. Dighe, and A. Mirizzi, “Signatures of collective and matter effects on supernova neutrinos at large detectors”, [arXiv:1008.0308](#).
- [80] **Hyper-Kamiokande Working Group** Collaboration, E. Kearns *et al.*, “Hyper-Kamiokande Physics Opportunities”, [arXiv:1309.0184](#).
- [81] H. Janka and E. Mueller, “Neutrino driven type II supernova explosions and the role of convection”, *Phys.Rept.* **256** (1995) 135–156.
- [82] K. Langanke and G. Martinez-Pinedo, “Nuclear weak interaction processes in stars”, *Rev.Mod.Phys.* **75** (2003) 819–862, [arXiv:nucl-th/0203071](#).
- [83] A. Mezzacappa, “Ascertaining the Core Collapse Supernova Mechanism: The State of the Art and the Road Ahead”, *Ann.Rev.Nucl.Part.Sci.* **55** (2005) 467–515.
- [84] A. Burrows, L. Dessart, C. D. Ott, and E. Livne, “Multi-Dimensional Explorations in Supernova Theory”, *Phys.Rept.* **442** (2007) 23–37, [arXiv:astro-ph/0612460](#).
- [85] H.-T. Janka, K. Langanke, A. Marek, G. Martinez-Pinedo, and B. Mueller, “Theory of Core-Collapse Supernovae”, *Phys.Rept.* **442** (2007) 38–74, [arXiv:astro-ph/0612072](#).
- [86] S. Woosley and T. Janka, “The physics of core-collapse supernovae”, *Nature Physics*, 2006 [arXiv:astro-ph/0601261](#).
- [87] A. Burrows, “Colloquium: Perspectives on core-collapse supernova theory”, *Rev.Mod.Phys.* **85** (2013) 245, [arXiv:1210.4921](#).
- [88] H.-T. Janka, “Explosion Mechanisms of Core-Collapse Supernovae”, *Ann.Rev.Nucl.Part.Sci.* **62** (2012) 407–451, [arXiv:1206.2503](#).
- [89] C. D. Ott, “The Gravitational Wave Signature of Core-Collapse Supernovae”, *Class.Quant.Grav.* **26** (2009) 063001, [arXiv:0809.0695](#).
- [90] K. Kotake, “Multiple physical elements to determine the gravitational-wave signatures of core-collapse supernovae”, *Comptes Rendus Physique* **14** (2013) 318–351, [arXiv:1110.5107](#).
- [91] S. Ando, B. Baret, I. Bartos, B. Bouhou, E. Chassande-Mottin, *et al.*, “Multimessenger astronomy with gravitational waves and high-energy neutrinos”, *Rev.Mod.Phys.* **85** (2013) 1401–1420, [arXiv:1203.5192](#).
- [92] H. Yuksel and M. D. Kistler, “The Cosmic MeV Neutrino Background as a Laboratory for Black Hole Formation”, [arXiv:1212.4844](#).
- [93] S. Woosley and J. Bloom, “The Supernova Gamma-Ray Burst Connection”, *Ann.Rev.Astron.Astrophys.* **44** (2006) 507–556, [arXiv:astro-ph/0609142](#).
- [94] S. Woosley, D. Hartmann, R. Hoffman, and W. Haxton, “The Neutrino Process”, *Astrophys.J.* **356** (1990) 272–301.
- [95] F. Thielemann, F. Brachwitz, C. Freiburghaus, E. Kolbe, G. Martinez-Pinedo, *et al.*, “Element synthesis in stars”, *Prog.Part.Nucl.Phys.* **46** (2001) 5–22, [arXiv:astro-ph/0101476](#).
- [96] A. Heger, E. Kolbe, W. Haxton, K. Langanke, G. Martinez-Pinedo, *et al.*, “Neutrino nucleosynthesis”, *Phys.Lett.* **B606** (2005) 258–264, [arXiv:astro-ph/0307546](#).
- [97] S. Woosley and A. Heger, “Nucleosynthesis and Remnants in Massive Stars of Solar Metallicity”, *Phys.Rept.* **442** (2007) 269–283, [arXiv:astro-ph/0702176](#).
- [98] M. D. Kistler, W. C. Haxton, and H. Yuksel, “Tomography of Massive Stars from Core Collapse to Supernova Shock Breakout”, *Astrophys. J.* **778** (2013) 81, [arXiv:1211.6770](#).
- [99] I. Gil Botella and A. Rubbia, “Oscillation effects on supernova neutrino rates and spectra and detection of the shock breakout in a liquid argon TPC”, *JCAP* **0310** (2003) 009, [arXiv:hep-ph/0307244](#).
- [100] I. Gil Botella and A. Rubbia, “Decoupling supernova and neutrino oscillation physics with LAr TPC detectors”, *JCAP* **0408** (2004) 001, [arXiv:hep-ph/0404151](#).